JOURNAL OF SUSTAINABLE MATERIALS PROCESSING AND MANAGEMENT
e-ISSN: 2821-2843

JSMPM

Vol. 5 No. 2 (2025) 83-93
https://publisher.uthm.edu.my/ojs/index.php/jsmpm

Electrosynthesis of Ni-Rich Cathode Materials for Li-Ion Batteries

T. N. Ardiansyah[1], A. Nur[1]*, A. Jazuli[1], M. H. A. Imam[1], Y. C. Danarto[1], A. Jumari[1], E. R. Dyartanti[1], A. W. Budiman[1], T. Paramitha[1], A. Purwanto[1]

[1] *Department of Chemical Engineering*
Universitas Sebelas Maret, Jl IR. Sutami 36 A, Surakarta, 57126, INDONESIA

*Corresponding Author: adriannur@staff.uns.ac.id
DOI: https://doi.org/10.30880/jsmpm.2025.05.02.007

Article Info

Received: 16 July 2025
Accepted: 3 October 2025
Available online: 30 October 2025

Keywords

Lithium-ion battery, NCA cathode, electrosynthesis, calcination temperature, cathode synthesis

Abstract

This study develops an electrosynthesis method for $LiNi_{0,89}Co_{0,08}Al_{0,03}O_2$ (NCA) cathode materials, utilizing water oxidation to generate hydroxide ions for precursor precipitation. Systematic characterization reveals calcination temperature critically governs morphology and performance: 600°C yields porous particles with residual hydroxides, 800°C produces dense, well-crystallized structures with optimal porosity, while 950°C causes over-sintering and Al segregation. FTIR analysis verified the successful formation of the precursor with distinct metal-oxygen vibrations. EDX shows temperature-dependent elemental distribution, with 800°C achieving ideal Ni/Co/Al integration. XRD confirms layered phase formation, and TG/DTA tracks thermal decomposition. Optimal conditions (1.5 A, 1 M concentration, 800 °C calcination) yield NCA cathodes with enhanced structural stability and electrochemical activity. The work demonstrates electrosynthesis as a sustainable, controllable route for high-performance NCA production.

1. Introduction

Lithium-ion (Li-ion) battery research is critical since this technology powers many contemporary devices, including electric cars, portable electronics, and energy storage for renewable sources [1,2]. The development of materials for lithium-ion batteries (LIBs) is underway, emphasizing cost-effectiveness, safety, long-term battery performance, and increased energy density. Some interesting LIB cathode materials that are presently being developed are NMC (Nickel Manganese Cobalt) - Ni-rich (NMC 811 and NMC 622), NCA (Nickel Cobalt Aluminum), LFP (Lithium Iron Phosphate), and Sulfur-Based Cathode (Li-S) [2,3]. Nickel-rich layered oxides, such as NCA and NMC, are widely used in lithium-ion batteries (LIBs) due to their high energy density and cost-effectiveness [4,5] While both NMC and NCA offer high capacity, they present distinct advantages and challenges. NMC materials, especially NMC 811, are widely studied for their good overall performance and thermal stability attributed to manganese integration [2,4]. In contrast, NCA cathodes often achieve a slightly higher specific capacity and better cycling stability due to the stabilizing role of aluminum, which suppresses detrimental phase transitions more effectively than manganese [4].

The NCA (Nickel Cobalt Aluminum) cathode material is synthesized using various methods to produce materials with the best properties. The Co-precipitation method, the solid-state reaction method, the sol-gel method, the flame spray pyrolysis method, and the hydrothermal method are all standard synthesis techniques utilized in the synthesis of NCA [4,5]. Co-precipitation is the most common industrial method for producing precursor materials with spherical morphology and homogeneous cation distribution. However, it requires precise control over pH, temperature, and stirring speed, often leading to complex and multi-step processes. Solid-

state reactions, while simpler, typically result in irregular particle shapes, poor homogeneity, and require high temperatures and long processing times, which can promote lithium loss and cation disorder [4]. These limitations of existing methods highlight the need for alternative synthesis routes that offer better control, simplicity, and efficiency. In this work, we developed a novel electrochemical process for the NCA cathode material synthesis. The exact control of structure and composition, energy efficiency, and environmental friendliness are the benefits of the electrochemical method.

2. Methodology

MERCK's nickel (II) sulfate heptahydrate, cobalt (II) sulfate heptahydrate, aluminum sulfate octa decahydrate, and sodium hydroxide are used. A 0.5M, 1M, or 1.5M solution of Ni:Co:Al with a mole ratio of 89:8:3 was stirred for thirty minutes at room temperature in a 250 mL beaker. This solution was adjusted to a pH 4 in the electrolysis cell using 4 M NaOH.

The two chambers of an electrochemical cell used to synthesize NCA were separated by a bipolar membrane (Fig. 1). To aid in homogenizing the solution, the 5 x 5 x 10 cm acrylic electrochemical cell was set up on an ultrasonic cleaner. Fumasep FBM, a bipolar membrane acquired from Fumatech BWT, was utilized. An anion exchange membrane faced the anode, while a cation exchange membrane faced the cathode in the configuration of the bipolar membrane. The anode and cathode were composed of 5x2 cm inert carbon. The power supply managed the current. Various currents of 1 A, 1.5 A, or 2 A were used. After the electrolysis procedure, the residue was neutralized in deionized water. After that, the residue was dried, and LiOH was added to the residue at a mole ratio 1:1.05 until the mixture was homogenous. After being heated for six hours at 500 ^{o}C, the precipitate mixture was calcined for twenty hours at 600 ^{o}C, 800 ^{o}C, 950 ^{o}C.

SEM/EDX, FTIR, TGDTA, and XRD were employed to analyze the samples. SEM/EDX analysis was performed using scanning electron microscopy. Examine S40, FEI using an acceleration voltage of 20 kV. Fourier Transformed Infrared Spectroscopy (FTIR Spectroscopy) (Shimadzu FTIR Spectrometer) was used to analyze the functional groups of samples. X-ray diffraction was employed to determine the particle's crystal structure. With a CuKα radiation source (α = 1.5406 Å) and a PanAnalytical, X' Pert Pro type, 30 kV scan step time was employed.

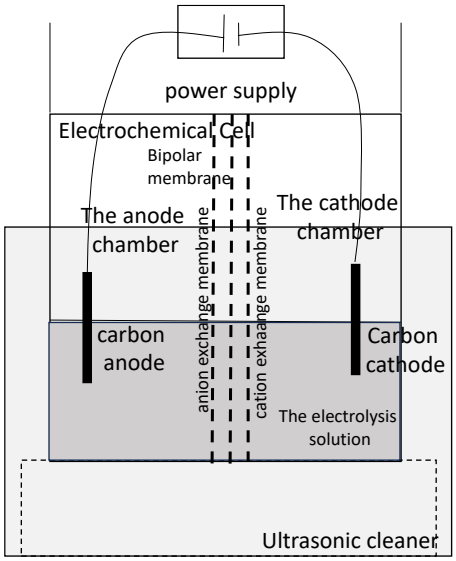

Fig. 1 *Electrosynthesis equipment for NCA Electrolysis*

3. Results and Discussion

3.1 SEM Analysis and Mechanism of Reaction

The SEM analysis results for every sample show a nearly identical picture (Fig. 2(d) and Fig. 2(e)). Agglomeration of primary particles between 0.5 and 1 μm results in the formation of larger particles. The calcination temperature variation is carried out to optimize the material distribution of NCA. Refer to Fig. 2 SEM images reveal that at 600°C, the particles appear homogeneous but contain wide cracks/pores, likely due to incomplete decomposition of precursors (e.g., sulfates/hydroxides) and gas release (e.g., SO_3) [6,7].

As the calcination temperature increases to 800°C, the SEM images show a dramatic improvement in particle morphology. The previously large pores and cracks significantly reduce in size, resulting in a more densely packed

J. of Sustainable Materials Processing and Management Vol. 5 No. 2 (2025) p. 83-93

structure with better interparticle connectivity. This transformation occurs due to complete precursor decomposition and enhanced sintering, where particles begin to coalesce and form stronger grain boundaries [5,8]. The optimized porosity at this temperature provides sufficient electrolyte infiltration channels while maintaining robust structural stability [9]. This balanced morphology explains why 800°C calcined NCA typically demonstrates superior electrochemical performance, offering both good lithium-ion diffusion pathways and excellent electronic conductivity through well-connected particle networks.[10].

At the extreme temperature of 950°C, while the material maintains low porosity, new morphological features emerge that may degrade performance. The SEM images reveal a layered or flaky surface structure, suggesting excessive sintering has occurred. This over-sintering leads to exaggerated grain growth and possible partial melting of particle surfaces [5]. Additionally, the high temperature may drive aluminum segregation to the surface, forming inactive Li-Al-O phases that block lithium-ion transport [5,11]. Although the dense structure appears favorable for electronic conduction, the reduced active material accessibility and potential cation mixing between lithium and nickel sites often result in diminished capacity and poorer rate performance compared to the 800°C sample [12,13]. These observations highlight the delicate balance required in calcination temperature selection for optimal NCA cathode performance.

The production of $LiNi_{0.89}Co_{0.08}Al_{0.03}O_2$ (NCA) via electrosynthesis begins with the electrochemical generation of hydroxide ions (OH^-) through water splitting. At the anode, water oxidizes to release oxygen, protons, and electrons, while the cathode reduces water to produce hydrogen gas and OH^- ions [14]. These hydroxide ions then react with dissolved nickel (Ni^{2+}), cobalt (Co^{2+}), and aluminum (Al^{3+}) salts, forming a mixed metal hydroxide precursor (Table 1) [4,15,16]. This precursor is later combined with lithium hydroxide (LiOH) and calcined at high temperatures (700–850°C) in an oxygen-rich environment to form the final layered NCA oxide structure. The process ensures precise control over composition and crystallinity critical for battery performance [17,18].

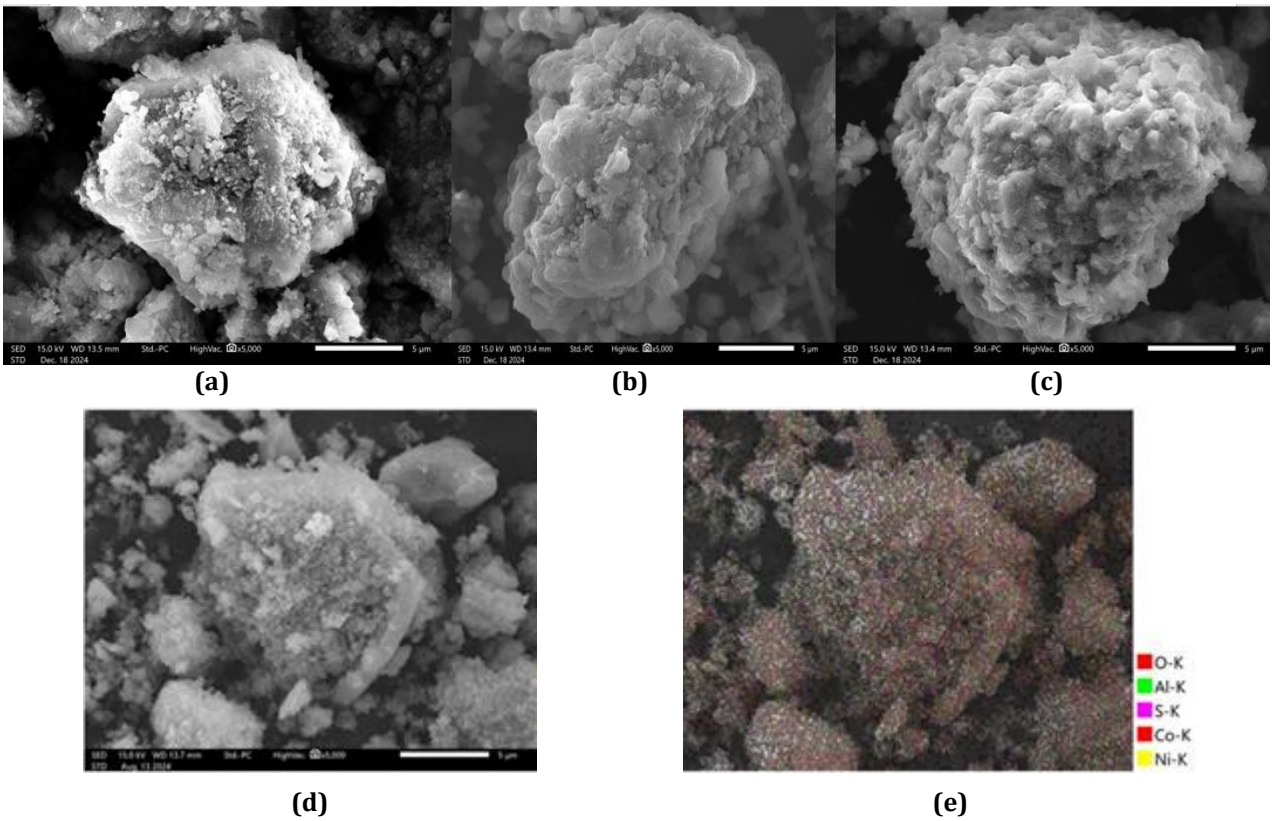

Fig. 2 *Morphology and distribution of elements at different temperatures of calcination within 1M of initial concentration at 1A: (a) 600°C, (b) 800°C, (c) 950°C, (d) Agglomeration of primary particles at 0.5 µm; and (e) at 1 µm both in 600°C calcination's temperature*

Several factors determine the success of NCA electrosynthesis. Current density must be carefully controlled too high and uneven precipitation occurs; too low and the reaction becomes inefficient [19]. Electrode stability is crucial, as anode materials like platinum or iridium oxide must resist corrosion during oxygen evolution [20]. The pH of the electrolyte (ideally 4-6) ensures uniform metal hydroxide precipitation without selective deposition

[21]. Additionally, solution mixing prevents localized concentration imbalances that could lead to non-stoichiometric particles. Finally, calcination conditions (temperature and oxygen flow) dictate the final crystal structure, with excessive heat risking lithium loss and cation disorder [18,22].

Table 1 *Mechanism of reaction*

Step	Description	Reaction Equation	Location / Note
(1)		Electrochemical Generation of OH^-	
(1a)	Anode Reaction (Water Oxidation)	$2H_2O\ (l) \rightarrow O_2\ (g) + 4H^+\ (aq) + 4e^-$	Anode Chamber
(1b)	Cathode Reaction (Water Reduction)	$4H_2O\ (l) + 4e^- \rightarrow 2H_2\ (g) + 4OH^-\ (aq)$	Cathode Chamber
(2)		Simultaneously Chemical Precipitation of Mixed Hydroxide Precursor	
(2a)	Precipitation Metal Hydroxide	$0{,}89Ni^{2+}\ (aq) + 0{,}08Co^{2+}\ (aq) + 0{,}03Al^{3+}\ (aq) + 2OH^-(aq) \rightarrow Ni_{0{,}89}Co_{0{,}08}Al_{0{,}03}(OH)_2\ (s)$	Bulk Solution / Cathode Chamber
(3)		Calcination to Form Layered NCA Oxide	
(3a)	Solid-State Reaction with Lithium	$2Ni_{0{,}89}Co_{0{,}08}Al_{0{,}03}(OH)_2\ (s) + 2{,}1LiOH\ (s) + 0{,}45O_2\ (g) \rightarrow 2LiNi_{0{,}89}Co_{0{,}08}Al_{0{,}03}O_2\ (s) + 5.1H_2O\ (g)$	Furnace (Post-electrosynthesis)

3.2 EDX Analysis

Energy-dispersive X-ray (EDX) analysis provides critical insight into how synthesis conditions affect compositional fidelity. The quantitative data for all samples are summarized in Table. 2. The influence of applied current was examined at a fixed initial metal ion concentration of 1.5 M. As shown in Fig. 3a, higher applied currents led to a decrease in Ni content and a relative increase in oxygen. For instance, as the current increased from 1 A to 2 A, the Ni content decreased from 20,79% to 2,79%, while the O content increased accordingly (Table. 2).

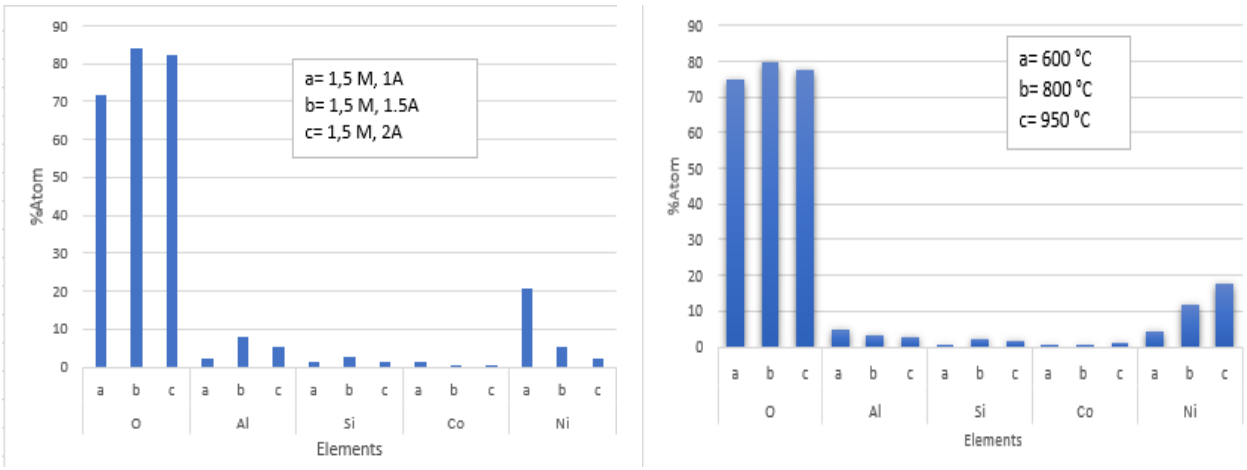

(a) **(b)**

Fig. 3 *(a) EDX of the sample showing quantitative results of 1.5M at various currents; (b) Main particles content sample 1M, 1.5A at different calcination's temperatures*

This suggests that excessively rapid OH^- generation at higher currents creates local pH gradients near the cathode surface [12]. These gradients can lead to non-uniform precipitation or slight oxidation of species at the electrode interface [23-26]. Under these conditions, the precipitation of metal hydroxides becomes extremely fast and potentially less controlled. It is possible that at excessively high precipitation rates, the formation of a less pure or non-stoichiometric precipitate is favored. Furthermore, the increased oxygen content is indicative of the formation of oxyhydroxide species (e.g., NiOOH) or greater adsorption of carbonate from the atmosphere (as CO_2 reacts with the basic solution), both of which are facilitated by a highly alkaline environment [12,26].

The effect of calcination temperature on elemental distribution was also profound. Fig. 3(b) shows the EDX data for samples calcined at different temperatures. At 600 °C, the analysis reveals significantly higher oxygen and aluminum content coupled with lower nickel and cobalt levels compared to samples processed at higher temperatures. As quantified in Table. 2, the O and Al contents at 600 °C were 5% and 75,09% respectively, which are markedly higher than those in the 800 °C sample. This compositional profile suggests incomplete phase transformation during the low-temperature treatment [25].

The elevated oxygen content indicates residual hydroxide or oxyhydroxide phases, while the high aluminum signal points to either unreacted Al_2O_3 or surface-segregated aluminum species that have not properly incorporated into the crystal lattice [25]. As the temperature increases to 800–950 °C, the particles become denser and smoother with fewer pores, indicating advanced sintering and improved crystallinity of the NCA structure [27]. Concurrently, EDX detects a decline in O and Al but a rise in Ni and Co, attributed to Al incorporation into the lattice and oxygen loss at higher temperatures [12,27]. While 800 °C yields an optimal balance of solid morphology and composition, 950 °C risks excessive Al volatilization and over-sintering, which may degrade electrochemical performance [28].

Table 2 *Detail of quantitative results for Fig. 3*

Synthesis condition	Ni (%)	Co (%)	Al (%)	O (%)	Other (%)
Current (1.5M)					
1.0 A	20.79	1.46	2.4	71.86	1.45
1.5 A	5.37	0.15	7.95	84.01	2.52
2.0 A	2.17	0.33	5.19	82.16	1.43
Calcination Temp.					
600 °C	4.42	0.25	0.25	75.09	0.6
800 °C	11.58	0.39	0.39	79.63	2.37
950 °C	17.45	1.06	1.06	77.51	1.43

3.3 FTIR Analysis

Fig. 4 shows the sample's FTIR spectra at different starting concentrations at 1.5M. The most significant feature for confirming the formation of the desired material is the absorption band emerging at ~600 cm^{-1}. This band is attributed to the stretching vibrations of metal-oxygen bonds (M-O, where M = Ni, Co) in the octahedral sites of the layered oxide structure [23,28,29]. A poorly defined M-O band might indicate disorder or the presence of inactive rock-salt phases like NiO, which block Li-ion diffusion paths and reduce specific capacity [23]. The band's intensity grows notably with increasing initial metal ion concentration (from 0.5 M to 1.5 M). This indicates that higher precursor concentrations promote the formation of a more developed oxide-like or oxyhydroxide-like local structure even before calcination [28]. This is consistent with the EDX data (Fig. 3(a)), which showed higher Ni content at higher concentrations, suggesting a more complete and possibly better-structured precipitation process.

The small absorption features in the region around 1200-1500 cm^{-1} can be tentatively assigned to C-O stretching vibrations from carbonate species (e.g., CO_3^{2-}) [30]. These are common contaminants in synthesized materials, often resulting from the absorption of atmospheric CO_2 by the basic hydroxide precipitate or from residual carbon-containing compounds [27]. While minor, the presence of surface carbonates is noteworthy for battery applications, as they can lead to gas evolution (CO_2) during the first charge and increase interfacial impedance, negatively impacting initial Coulombic efficiency. The sharp band observed at approximately 1600 cm^{-1} is assigned to the bending (scissoring) mode of adsorbed water molecules (H-O-H) [12,27]. This further corroborates the hydrophilic nature of the precursor material and aligns with the O-H stretching observation [12]. The broad and intense band in this region (3600 cm^{-1}) is characteristic of the O-H stretching vibration from hydroxyl groups (-OH) [12,31].

The FTIR analysis confirms the effective electrosynthesis of a mixed transition metal hydroxide precursor. The clear M-O vibration band indicates that the electrochemical precipitation method produces a material with

incipient structural order. The dependence of this band's intensity on initial concentration provides a valuable process optimization parameter. Higher concentrations within the studied range yield a chemically superior precursor, which is expected to translate into a higher-quality final NCA cathode after calcination. The presence of adsorbed water and potential carbonate contamination highlights critical considerations for the handling, storage, and subsequent processing (e.g., drying, calcination atmosphere) of the precursor to ensure the best possible electrochemical performance in the final battery cell [31,32].

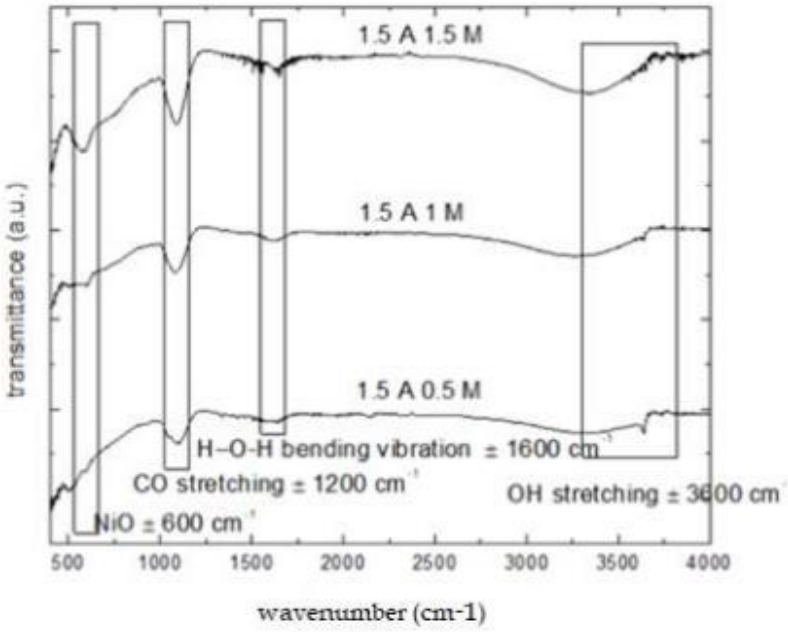

Fig. 4 *FTIR spectra of samples at 1.5 A and various initial concentrations*

3.4 TG/DTA Analysis

Thermogravimetric (TGA) and Differential Thermal Analysis (DTA) were employed to investigate the thermal stability and decomposition pathway of the as-synthesized Ni-Co-Al$(OH)_2$ precursor (prepared at 1.5 M and 2 A). The sample's thermal analysis curve at 1.5 M and 2 A at 0–1100 °C is shown in Fig. 5 the TGA curve shows the four stages of weight loss, while the DTA graph shows two endothermic peaks in tandem with them. The first weight loss, identified as area I, occurs between ambient temperature and 120 °C and is around 20 wt%. The endothermic peak in the DTA curve supports this observation and may be related to the hydroxyl groups being removed or water molecules vaporizing [33,34] Region III (400-600 °C) shows only minor weight loss. The corresponding endothermic DTA peak may be related to the thermal decomposition of $Ni(OH)_2$[35].

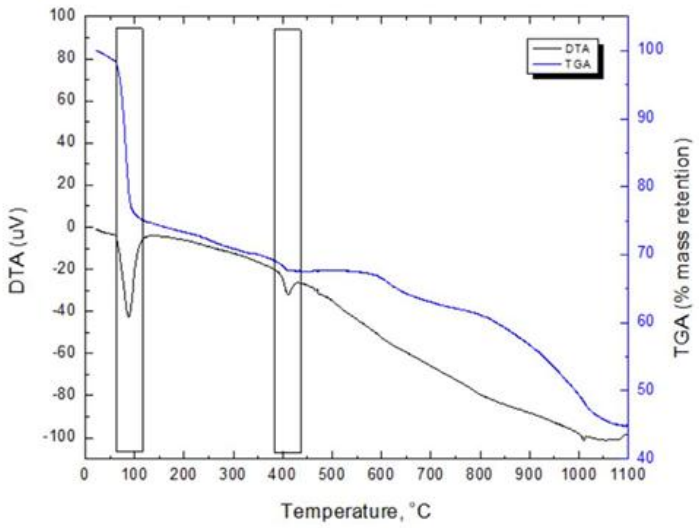

Fig. 5 *TG/DTA profile of sample preparation at 1.5 M and 2 A*

J. of Sustainable Materials Processing and Management Vol. 5 No. 2 (2025) p. 83-93

Region IV (>700°C) shows no significant mass loss is observed beyond 700°C. This is a pivotal finding, the flatness of the TGA curve indicates that mass loss reactions are complete by approximately 700°C. The small, broad features in the DTA curve above this temperature are not associated with mass loss and are instead attributed to crystallization and phase formation energy. These are likely exothermic events related to grain growth and sintering of the primary particles into the secondary spherical morphologies observed in SEM [31]. Crucially, the isothermal mass profile above 700°C indicates that calcination at 800°C minimizes the risk of lithium oxide (Li_2O) volatilization, which becomes significant at temperatures exceeding 900°C and leads to detrimental cation mixing (Ni^{2+} occupying Li^+ sites) [4,31].

This TG/DTA profile provides essential justification for our calcination temperature selection. The isothermal mass profile above 700°C indicates that calcination at 800°C is sufficient to achieve complete crystallization into the desired phase, as our XRD data confirms, while minimizing the risk of lithium oxide (Li_2O) volatilization [10]. This volatilization becomes significant at temperatures exceeding 900°C and leads to detrimental cation mixing (Ni^{2+} occupying Li^+ sites), which degrades electrochemical performance [4,31]. This thermal evidence aligns perfectly with our SEM and EDX observations, which showed that calcination at 950°C caused over-sintering and Al segregation, further validating 800°C as the optimal calcination temperature.

3.5 XRD Analysis

The X-ray diffraction pattern of the NCA particle is shown in Fig. 6 The diffraction pattern on JCPDS card 87-1562 matches the standard for $LiNiO_2$ (JCPDS card 87-1562), confirming the formation of the desired isostructural NCA [4,25,36]. A few of the peaks do not conform to the typical diffraction pattern. A comparison of the diffraction patterns before and after calcination is also displayed. Some sloping peaks suggest a match with the NCA diffraction pattern, but it is also clear that the uncalcined NCA diffraction pattern is amorphous and crystal-free [37]. During calcination, NCA particle crystals are produced.

The diffractogram of the as-synthesized material is characterized by broad, low-intensity humps with no sharp Bragg peaks. This amorphous-like pattern is typical of poorly crystalline mixed transition metal hydroxides, $Ni_{0.89}Co_{0.08}Al_{0.03}(OH)_2$ [33]. The lack of crystallinity confirms that the electrochemical synthesis produces a precursor that requires high-temperature treatment to achieve long-range atomic order. After calcination, all the diffraction peaks can be exclusively indexed to a layered hexagonal α-$NaFeO_2$ structure with the R-3m space group, confirming the successful formation of $LiNi_{0,89}Co_{0,08}Al_{0,03}O_2$ [4]. The absence of any extraneous peaks particularly between 20° and 25° 2θ where common impurity phases like NiO or $Li_xNi_{1-x}O$ appear demonstrates high phase purity. This indicates that the electrosynthesis method, followed by optimized calcination, effectively incorporates Co and Al into the lattice and prevents the formation of isolated secondary phases [4,38]

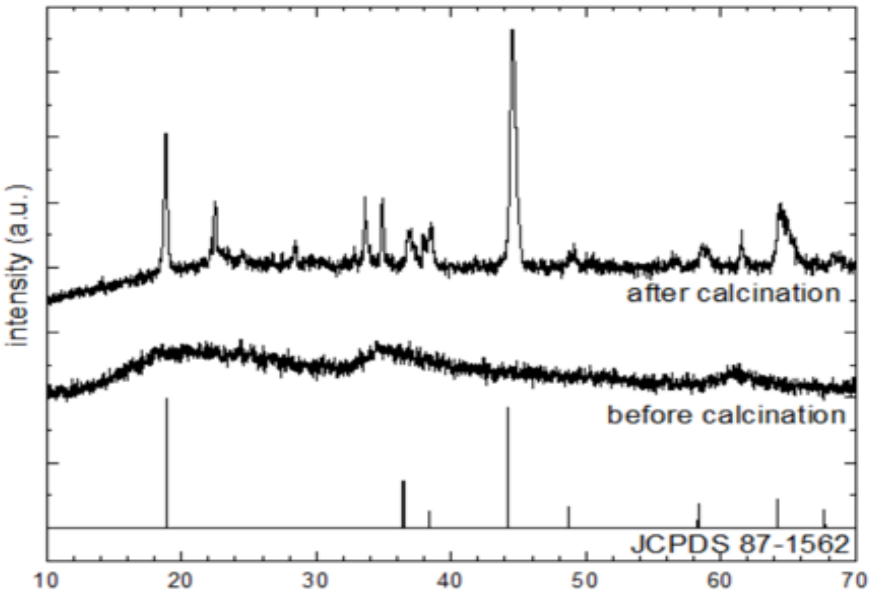

Fig. 6 *NCA XRD sample before and after calcination*

After calcination, all diffraction peaks index exclusively to a layered hexagonal α-$NaFeO_2$ structure (R-3m space group), confirming the successful formation of $LiNi_{0.89}Co_{0.08}Al_{0.03}O_2$. The diffraction pattern originates from the periodic crystal lattice [28]. Given nickel's dominance (89%), the pattern primarily reflects the Ni-O

framework, with Co and Al atoms incorporated substitutionally into nickel sites. The absence of separate peaks for secondary phases like NiO, Co_3O_4, or Al_2O_3 evidences this successful incorporation and demonstrates high phase purity [28,35]. This indicates that the electrosynthesis method, followed by optimized calcination, effectively incorporates Co and Al into the lattice and prevents the formation of isolated secondary phases [28].

A well-ordered layered structure is evidenced by the clear separation (splitting) of the peaks for the (006)/(102) and (108)/(110) planes [4]. As seen in Fig. 6, these doublets are distinctly resolved in our sample calcined at 800°C. This splitting is a sensitive indicator of low cationic mixing, a phenomenon where Ni^{2+} ions (0.69 Å) migrate from the transition metal (3a) sites to the lithium (3b) sites due to their similar ionic radii. High cationic mixing disrupts the Li^+ diffusion channels, leading to poor rate capability and capacity fade. The clear separation observed confirms that our synthesis process successfully minimizes this disorder. The intensity ratio between the (003) and (104) peaks is a widely used metric to quantify cationic disorder. A ratio greater than 1.2 is generally considered indicative of a well-ordered layered structure with low Ni^{2+} occupancy in the Li layer [15]. For our 800 °C sample, the I(003)/I(104) ratio was calculated to be approximately 0.7. While this value is below the ideal threshold of 1.2 and suggests a degree of cation mixing. The clear separation of the (006)/(102) and (108)/(110) peaks confirm a well-defined layered structure. Therefore, the overall structural quality remains high, and minimizing this residual cation mixing presents an opportunity for further optimization of the synthesis or calcination process [10,23,25,39].

4. Conclusion

This study successfully demonstrates the novel electrosynthesis of $LiNi_{0.89}Co_{0.08}Al_{0.03}O_2$ (NCA) cathode material, presenting an alternative to conventional methods like co-precipitation and solid-state reaction. The primary objective was to determine the influence of initial metal ion concentration and applied current on the synthesis process and final material properties. Our findings clearly show that these parameters are critical for achieving optimal composition and structure. The initial metal ion concentration directly influenced the precursor quality, with a 1.5 M solution yielding the highest Ni content and most developed metal-oxygen bonding structure, as confirmed by EDX and FTIR. Regarding the applied current, a value of 1.5 A was found to be optimal; lower currents led to inefficient synthesis, while higher currents 2 A caused non-uniform precipitation and off-stoichiometry due to localized pH gradients. Most significantly, systematic investigation of calcination temperature established 800°C as the optimal condition, producing NCA particles with a dense, well-crystallized morphology, ideal elemental distribution, and a phase-pure layered structure that minimizes cation mixing. The key novelty of this research lies in the application of a direct electrochemical method to generate hydroxide ions for the precipitation of the NCA precursor. This approach offers precise control over composition, simplifies the synthesis process by eliminating complex pH stat systems, and aligns with green chemistry principles by using water as a reactant. Therefore, this work establishes electrosynthesis as a sustainable, controllable, and efficient route for producing high-performance NCA cathode materials.

Acknowledgement

This work was supported by Universitas Sebelas Maret (UNS).

Conflict of Interest

Authors declare that there is no conflict of interests regarding the publication of the paper.

Author Contribution

The authors confirm contribution to the paper as follows: ***study conception and design:*** *A. Nur, T.N Ardiansyah;* ***data collection:*** *T.N. Ardiansyah, A. Jazuli, Imam M.H.A;* ***analysis and interpretation of results:*** *T.N. Ardiansyah, A. Jazuli, Imam M.H.A, A. Nur;* ***draft manuscript preparation:*** *T.N. Ardiansyah, A. Jazuli, Imam M.H.A, A. Nur, Y.C Danarto, A. Jumari, E.R. Dyartanti, A.W. Budiman, T. Paramitha, A. Purwanto. All authors reviewed the results and approved the final version of the manuscript.*

References

[1] Amuta, O., Yao, J., Droese, D., & Kowal, J. (2025). Accurate Chemistry Identification of Lithium-Ion Batteries Based on Temperature Dynamics with Machine Learning. Batteries, 11(6), 208. https://doi.org/10.3390/batteries11060208

[2] Chowdhury, S., Barrera, A., Marinova, M., Fadel, A., Bellayer, S., Hosdez, J., ... & Maschke, U. (2025). Impact of external short circuit on lithium-ion batteries: a post-mortem case study. *Journal of Materials Chemistry A*, 13(24), 18600-18609. https://doi.org/10.1039/d5ta00705d

[3] Lv, L., Zhou, S., Liu, C., Sun, Y., Zhang, J., Bu, C., ... & Huang, Y. (2024). Recycling and reuse of spent LIBs: Technological advances and future directions. *Molecules*, 29(13), 3161. https://doi.org/10.3390/molecules29133161

[4] Purwamargapratala, Y., Zulfia, A., Kartini, E., Sukirman, E., Rois, M. F., Jodi, H., ... & Hardian, M. (2025). Synthesis and characterization of LiNi0. 5Mn0. 4Co0. 1O2 as a cathode material for lithium-ion batteries using the coprecipitation method. *Chemical Papers*, 1-10. https://doi.org/10.1007/s11696-025-04144-y

[5] Oh, Y., Kim, H., Lim, J., Hwang, Y., Jo, S., You, H., ... & Lim, J. (2025). Enhanced Electrical Connectivity in High Energy Density Single-Crystal NCA Electrodes via Polycrystalline Blending Design. *ACS Applied Materials & Interfaces*, 17(19), 28094-28102. https://doi.org/10.1021/acsami.5c01515

[6] Yu, S., Mao, Y., Xie, J., Xu, C., & Lu, T. (2024). Thermal runaway chain reaction determination and mechanism model establishment of NCA-graphite battery based on the internal temperature. *Applied Energy*, 353, 122097. https://doi.org/10.1016/j.apenergy.2023.122097

[7] Hu, S., Wang, J., Lu, Y., Yang, L., Xiong, L., Zhao, S., ... & Yang, Y. (2022). An epitaxial coating with preferred orientation stabilizing High-Energy Ni-Rich NCA cathodes. *Applied Surface Science*, 579, 152183. https://doi.org/10.1016/j.apsusc.2021.152183

[8] Li, W., Lee, S., & Manthiram, A. (2020). High‐nickel NMA: a cobalt‐free alternative to NMC and NCA cathodes for lithium‐ion batteries. *Advanced materials*, 32(33), 2002718. https://doi.org/10.1002/adma.202002718

[9] Amarray, A., Boutahar, A., El Fallah, H., Silvère, K. T., Bendali, A. E., Boutajanouit, L., ... & Dahbi, M. (2024). Recovery of lithium from spent LFP and NCA batteries by electro-oxidation process and synthesis of cathode material from recycled precursors. *Journal of Energy Storage*, 102, 114001. https://doi.org/10.1016/j.jpowsour.2022.231589

[10] González-Aguilera, L., Vicent-Luna, J. M., Ferrer, M. L., del Monte, F., & Gutiérrez, M. C. (2025). DES-based leachates containing LCO, NMC or NCA oxides as electrolytes for 2.2 V supercapacitors. *Chemical Engineering Journal*, 506, 159839. https://doi.org/10.1016/j.est.2024.114001

[11] Zhang, L., Huang, L., Zhang, Z., Wang, Z., & Dorrell, D. D. (2022). Degradation characteristics investigation for lithium-ion cells with NCA cathode during overcharging. *Applied Energy*, 327, 120026. https://doi.org/10.1016/j.cej.2025.159839

[12] Guo, B., He, R., Li, Y., Zhou, S., Zhang, L., Liu, X., & Yang, S. (2024). Aging mechanisms of cylindrical NCA/Si-graphite battery with high specific energy under dynamic driving cycles. *Journal of Energy Storage*, 103, 114287. https://doi.org/10.1016/j.est.2024.114287

[13] Liu, X., Lv, N., Du, P., Zhang, Y., Zhu, X., & Wang, Y. (2025). An SiO2 electrochemical microcell enabled composite solid electrolyte for stable lithium metal battery. *Journal of Alloys and Compounds*, 1012, 178503. https://doi.org/10.1016/j.jallcom.2025.178503

[14] Bayri, A., Gocer, E., Altin, E. M. İ. N. E., Altundag, S. E. B. A. H. A. T., Oz, E., Harfouche, M., ... & Avci, S. E. V. D. A. (2020). LiNi0. 8Co0. 15Ti0. 05O2: synthesis by solid state reaction and investigation of structural and electrochemical properties with enhanced battery performance. *Journal of Materials Science: Materials in Electronics*, 31(22), 20527-20538. https://doi.org/10.1007/s10854-020-04572-4

[15] Kim, S., Park, S., Kim, D., Kim, C., Koo, N., Kim, J., & Kwon, K. (2024). Closed-loop resynthesis of LiNiCoAlO2 cathode active materials from the industrial leachate of spent li-ion batteries. *Chemical Engineering Journal*, 494, 153199. https://doi.org/10.1016/j.cej.2024.153199

[16] Hussain, S., Katkar, P. K., Vikraman, D., Sheikh, Z. A., Nazir, G., Batoo, K. M., ... & Jung, J. (2023). Direct and Binder‐Free MXene‐Assisted Cobalt Manganese Phosphate Electrode Fabrication on Carbon Cloth by Electrosynthesis for Efficient Supercapacitors. *International Journal of Energy Research*, 2023(1), 6653784. https://doi.org/10.1155/2023/6653784

[17] Li, S., Zhou, Y., Li, K., Saccoccio, M., Sažinas, R., Andersen, S. Z., ... & Chorkendorff, I. (2022). Electrosynthesis of ammonia with high selectivity and high rates via engineering of the solid-electrolyte interphase. *Joule*, 6(9), 2083-2101. https://doi.org/10.1016/j.joule.2022.07.009

[18] Li, Y., Ge, J., Zhu, J., Huang, G., Liu, C., Ge, Y., ... & Liu, H. (2025). Intermetallic PtSn Nanosheets with p–d Orbital Hybridization for Selective Hydroxylamine Electrosynthesis. *ACS nano*, 19(10), 10489-10499.

[19] Hu, Q., Yang, K., Peng, O., Li, M., Ma, L., Huang, S., ... & Loh, K. P. (2023). Ammonia electrosynthesis from nitrate using a ruthenium–copper cocatalyst system: a full concentration range study. *Journal of the American Chemical Society*, 146(1), 668-676.

[20] Li, S., Zhou, Y., Li, K., Saccoccio, M., Sažinas, R., Andersen, S. Z., ... & Chorkendorff, I. (2022). Electrosynthesis of ammonia with high selectivity and high rates via engineering of the solid-electrolyte interphase. *Joule*, 6(9), 2083-2101. https://doi.org/10.1038/s41586-022

[21] Ji, H., Zhao, Z., Zhang, C., & Li, X. (2024). In situ electrosynthesis of quinone-based redox-active molecules coupling with high-purity hydrogen production. *Chemical Science*, 15(33), 13185-13190. https://doi.org/10.1039/d4sc03033h

[22] Matras, D., Ashton, T. E., Dong, H., Mirolo, M., Martens, I., Drnec, J., ... & Vamvakeros, A. (2022). Emerging chemical heterogeneities in a commercial 18650 NCA Li-ion battery during early cycling revealed by synchrotron X-ray diffraction tomography. *Journal of Power Sources*, 539, 231589. https://doi.org/10.1016/j.jpowsour.2022.231589

[23] Xie, K., Liu, X., Xia, K., Diao, L., Lu, P., Wang, M., ... & Zhang, X. (2024). Innovative Mn3− xO4− y@ NCA design: Leveraging Mn/O vacancies and amorphous architecture for enhanced sodium-ion storage. *Journal of Energy Chemistry*, 97, 747-756. https://doi.org/10.1016/j.jechem.2024.06.059

[24] Park, G. T., Ryu, J. H., Kim, J. H., Sun, H. H., Suh, D. E., Han, S. M., ... & Sun, Y. K. (2024). Aluminum-distribution-dependent microstructural evolution of NCA cathodes: Is aluminum homogeneity really favorable?. *Energy Storage Materials*, 70, 103496. https://doi.org/10.1016/j.ensm.2024.103496

[25] Zhou, W., Li, X., Cui, S., Shao, Z., Cui, Y., & Zhang, W. (2023). A facile homogeneous precipitation route synthesis of LiNi1/3Co1/3Mn1/3O2 cathode material for lithium-ion batteries. *International Journal of Electrochemical Science*, 18(3), 100027. https://doi.org/10.1016/j.ijoes.2023.01.027

[26] Yuan, Y., Ma, Q., Zhang, X., Zhang, F., Song, X., Xin, H., ... & Zhang, H. (2024). Influence of cathode materials on thermal characteristics of lithium-ion batteries. *Frontiers in Chemistry*, 12, 1324840. https://doi.org/10.3389/fchem.2024.1324840

[27] Chen, Z., Hou, B., Zhang, M., Wang, Y., Peng, H., Dou, R., ... & Liu, X. (2026). Study on gas diffusion during the calcination of LiNi0. 8Co0. 1Mn0. 1O2 cathode materials. *Journal of the Taiwan Institute of Chemical Engineers*, 178, 106364. https://doi.org/10.1016/j.jtice.2025.106364

[28] Dong, Y., Zhai, H., Gao, Z., Gong, G., & Li, F. (2025). Study on the preparation of calcium modified coal gangue and its adsorption performance of phosphate. *Scientific Reports*, 15(1), 2240. https://doi.org/10.1038/s41598-025-86435-8

[29] Hossain, R., & Sahajwalla, V. (2022). Microrecycled Co3O4 from waste lithium-ion battery: synthesis, characterisation and implication in environmental application. *Journal of Environmental Chemical Engineering*, 10(3), 107858. https://doi.org/10.1016/j.jece.2022.107858

[30] Zhou, H., Gu, Z., Li, M., Fan, M., Zhao, Z., Fu, S., & Wang, K. (2025). SEM characterization technique for air-sensitive all-solid-state lithium battery materials. *Ultramicroscopy*, 114194. https://doi.org/10.1016/j.ultramic.2025.114194

[31] Wang, Q., Wang, Z., Li, X., Zhu, Y., & Gao, P. (2023). Synthesis and characterization of Co-free NMA cathodes for fast charging lithium-ion batteries. *Journal of Alloys and Compounds*, 955, 170226. https://doi.org/10.1016/j.jallcom.2023.170226

[32] Babaei, E., Bazyari, A., Shojaei, B., & Thompson, L. T. (2025). Nanostructured iron and nickel oxide aerogels revolutionizing asphaltene removal in hydrocarbon processing. *Scientific Reports*, 15(1), 12729. https://doi.org/10.1038/s41598-025-95667-7

[33] Zafari, M., & Shariatmadar Tehrani, F. (2025). Enhanced photocatalytic performance of non-stoichiometric WO3− x nanocrystals via near-infrared localized surface plasmon resonance. *Scientific Reports*, 15(1), 14624. https://doi.org/10.1038/s41598-025-99138-x

[34] Zahra, S., Naz, U., Irshad, M., Sheikh, A., & Zahra, S. (2025). Effect of calcination temperature on structural and magnetic properties of polypropylene glycol stabilized nickel ferrite nanoparticles. *BMC chemistry*, 19(1), 106. https://doi.org/10.1186/s13065-025-01454-w

[35] Elmaataouy, E., Kouchi, K., Chari, A., Alami, J., & Dahbi, M. (2023). Recycling of NCA cathode material from end-of-life LiBs via Glycerol-triacetate solvent-based separation. *Journal of Power Sources*, 587, 233702. https://doi.org/10.1016/j.jpowsour.2023.233702

[36] Abdelhalim, J. O., Amer, I., Abdel Latif, I., Fawzy, I., Ismail, S., & Khalaf, M. A. (2025). Investigation of the optimum calcination temperature for water treatment plant sludge to develop a sustainable alkali activated concrete. *Scientific Reports*, 15(1), 2117. https://doi.org/10.1038/s41598-025-85225-6

[37] Cho, M., Lee, S. H., Yuk, E., Park, H., & Kim, S. H. (2023). Nanoscale electrical characterization of ambient-induced surface impurities on high-nickel cathode materials for lithium-ion batteries. Journal of Alloys and Compounds, 963, 171215. https://doi.org/10.1016/j.jallcom.2023.171215

[38] Parker, J., Smith, R., & Cumming, D. (2024). High-resolution X-ray mapping of fluorinated binders in lithium-ion battery electrodes. *The Journal of Physical Chemistry C*, 128(49), 20957-20966. https://doi.org/10.1021/acs.jpcc.4c05678